Pergamon

Int. J. Solids Structures Vol. 31, No. 22, pp. 3079–3098, 1994

0020–7683/94 $7.00 + .00

0020–7683(94)E0064–3

QUASI-IMPACT DAMAGE INITIATION AND GROWTH OF THICK-SECTION AND TOUGHENED COMPOSITE MATERIALS

SHENG LIU
Department of Mechanical and Aerospace Engineering, Florida Institute of Technology, Melbourne, FL 32901, U.S.A.

(*Received* 24 *January* 1994; *in revised form* 8 *April* 1994)

Abstract—Results are presented for a study of damage initiation and growth in thick-section and toughened continuous fiber-reinforced composites resulting from a spherical indenter/impactor. The proposed analytical/computational model consists of several sub-models. A three-dimensional mesh generator is used for generating initial meshes for laminated composites containing various matrix cracks and delaminations. A stress analysis is developed in the framework of finite deformation for calculating stresses and strains of the composites with and without internal damage. A robust contact analysis proposed for handling the contact condition of cracked interfaces for matrix cracks/delaminations induced during indentation loading. A failure analysis is developed for predicting the damage initiation and propagation. A fracture mechanics based, simplified criterion is proposed for predicting the critical load for delamination growth.

The proposed model predicts that the damage of thick-section composites may be initiated from the layer right below the indenter due to the compressive load, or the interior shear matrix cracks due to transverse shear. This contradicts the conclusions for thin, brittle laminated composites, in which surface cracking is in general the initial damage mode. It is shown that the delamination induced by the shear cracks is dominated by fracture modes II and III for growth of thick-section composites due to indentation loading. It is also interesting to observe that complicated contact zone exists for different delaminations.

1. INTRODUCTION

Due to recent advances in design and manufacturing, advanced fiber-reinforced composites have been adopted more and more for the design of light-weight aerospace and aircraft structures. The design of the proposed National Aerospace Plane and Space Stations would undoubtedly be required to use these materials. The newest Boeing 777 tail part is expected to be made of advanced composite materials. New generation submarines also require the use of advanced composites. The applications of composite materials to human implants such as hip stems are also increasing. As a result, thicker and thicker composite structures are being used in primary load carrying structures such as wing roots as well as in aircraft engine fan blades.

One of the major problems in designing advanced composite materials for structural application is the vulnerability of the materials to transverse impact which can cause significant internal damage in terms of matrix cracking and delamination. It has been observed that the compressive strength of composites after impact (CAI) could be reduced significantly due to the extensive internal damage resulting from the impact. The design allowables are much lower than undamaged composite plates and therefore designs are fairly conservative. The matrix cracking and delamination is invisible to the naked eye and therefore forms an important reliability concern for aircraft, aerospace and other advanced systems.

Because of the significance of the problem, numerous experimental and analytical investigations have been performed to study the damage resulting from transverse loads, as shown by a pioneer work by Malvern *et al.* (1978) and two recent review articles by Abrate (1991) and Cantwell and Morton (1991). The analytical work previously developed has mostly emphasized estimating the overall delamination sizes and has been limited mostly to brittle systems and thin plates [Choi *et al.* (1991a, b); Gosse and Mori (1988); Gu and Sun (1987); Jones *et al.* (1988); Joshi and Sun (1986); Liu and Malvern (1987);

Poe (1988); Sjöblom *et al.* (1988); Wu and Springer (1988a), to name a few]. Although these models provide reasonable estimates of the damage size, the mechanics of damage growth and the material behavior during impact cannot be obtained from these models. None of these mentioned models addresses the detailed fracturing process during the formation and growth of the damage.

Recent studies on the impact or quasi-impact damage [Liu *et al.* (1991a, b, 1993); Liu (1992); Liu and Chang (1993); Martin and Jackson (1991); Salpekar (1991); Sun and Manoharan (1989), to name a few] have shown that the extent of delamination strongly depends upon the location of the initial matrix cracks and there is a strong interaction between matrix cracking and delamination growth (Liu *et al.*, 1991a, b; Liu, 1992; Liu and Chang, 1993). The matrix cracking has been proven quantitatively (Liu *et al.* 1991a, b; Liu, 1992) to be the initial damage mode and delamination is induced by the transverse matrix cracking. Computer simulation of the damage initiation to the final collapse of the structure was compared with the experimental data. Depending on the location of the matrix cracking, the delamination growth can be stable or unstable and can be dominated by different fracture modes. However, the existing findings are limited to thin, brittle laminated composites.

At the same time, efforts have been put forth on improving the toughness of composite materials such as introducing high strain-to-failure fibers, tougher resin systems and the use of compliant layers in between certain plies of the laminate. Therefore, the damage mechanics and mechanisms are expected to be complicated and could be different from those found for brittle material systems. Depending on different toughening mechanisms, the fracture resistance can show significant differences. Generally speaking, the fracture toughness for toughened systems is much larger than traditional brittle thermoset systems. However, the fracture modes contribution to the fracture is different. For example, the mode I and mode II fracture toughness of APC-2 are almost equal. The toughened thermoset systems have demonstrated improvement in mode II fracture toughness. The stitched systems generally have a bigger improvement in mode I. A newer composite system, T800H/3900-2 [see Odagiri *et al.* (1989)], has been reported to have a large improvement in both modes I and II fracture toughness. This material system is toughened on the interface with small polymide particles in the level of prepreg and therefore is a cost-effective way in terms of manufacturing cost and quality. Initial experimental data by Liu and Chang (1993) showed that the quasi-impact damage sizes for T800H/3900-2 laminates are significantly smaller than those for T300/976 laminates when the impact energy, the impactor size and plate geometries were kept unchanged. It is interesting to note that the strength and stiffness data are similar for T300/976 and T800H/3900-2 systems, while the fracture toughness for T800H/3900-2 is significantly higher.

It is therefore concluded that impact damage tolerance for toughened laminates could be improved over brittle laminates and it is believed that the fracture toughness contributes to the difference observed for different damage sizes. The question, however, arises as to what fracture mode(s) dominate under such imposed conditions. Another important consideration is that the damage modes for thick composites could be different from thin ones under impact loading. For thin laminates, it seems that the structural response plays an important role in the damage initiation and growth, while for thick composites, local material response may dominate the impact energy transfer. The initial damage mode for thin plates under impact load is always the surface matrix cracking due to global plate bending [see Finn and Springer (1991); Liu *et al.* (1991a, b, 1993); Liu (1992); Liu and Chang (1993)]. However, the initial damage mode for thick composites could be the crushing below the indenter or internal shearing crack inside the laminate (Finn, 1991). It is expected that damage growth due to different initial damages could be different for thin and thick composites. Unfortunately, no systematic research has been presented.

Accordingly, this paper presents an analytical model to understand the damage mechanics of laminated composites subjected to transverse concentrated loading for thick-section and toughened composites due to transverse concentrated loading. The proposed analytical/numerical model is capable of simulating the response of laminated composites with or without initial damage to transverse loading. Specifically a nonlinear finite element

model is adapted (Liu, 1992; Liu and Chang, 1993) for stress analysis. Appropriate failure criteria are used to predict initial damage. A rigorous contact mechanics model is developed to help prevent matrix crack and delamination interfaces from overlapping. A fracture mechanics model is utilized to predict when and how the cracks and delaminations grow. Due to the difficulty of numerical modeling, only cross-ply laminated composite panels are studied, and the load is assumed to be applied quasi-statically.

2. STATEMENT OF PROBLEM

Consider a cross-ply laminated composite plate subjected to a quasi-static transverse concentrated loading as shown in Fig. 1. The rectangular plates could be simply supported or clamped on any one of the edges and subjected to a transverse quasi-static concentrated load by a spherical indenter. It is desirable to obtain the following:

(1) the initiation of matrix cracking and the corresponding load;
(2) delamination initiation and propagation;
(3) extent of delamination as a function of the applied load;
(4) the fracture modes contributing to the delamination growth;
(5) the contact information associated with the delamination growth.

The first problem was to find the initial damage in terms of location and type by several existing failure criteria. After the initial damage was identified, the plates were assumed to contain a small delamination located at the central loading area on a 90/0 interface directly beneath the indenter, attached to the initial crack(s). Two types of matrix cracking in conjunction with the delamination were considered in the study; a bending crack and a pair of shear cracks. Accordingly, for a given loading and boundary condition, four types of internal damage modes were studied: (1) delamination with no matrix cracks; (2) delamination induced by a bending crack; (3) delamination induced by shear cracks; (4) delamination induced by both a bending crack and a pair of shear cracks as shown in Fig. 2.

3. METHOD OF APPROACH

3.1. *Stress analysis*

As the local deformations of the laminate could be substantial due to the concentrated load, finite deformation theory was adopted in the analysis. The total potential energy Π of a laminate without damage under the given load can be described as

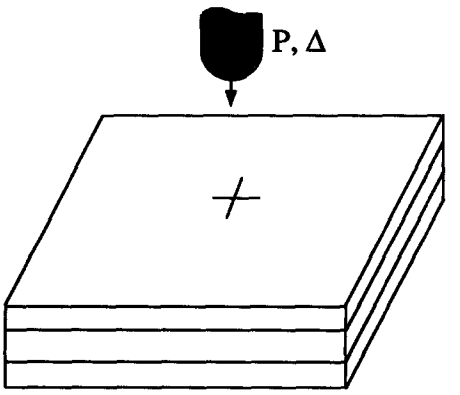

Fig. 1. Description of the problem. A laminated composite panel subjected to a transverse load applied by a spherically-nosed indenter.

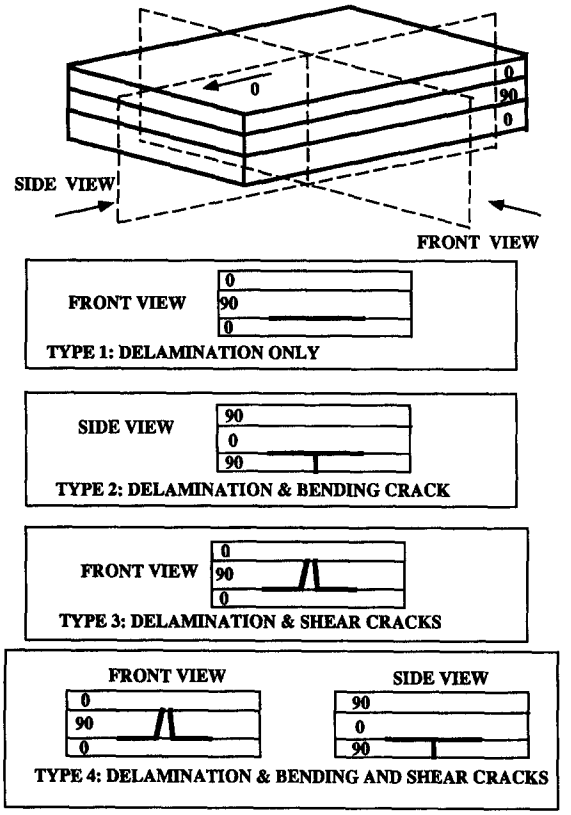

Fig. 2. Four types of damage modes considered in this analysis: (1) delamination with no matrix cracks; (2) delamination induced by a bending crack; (3) delamination induced by shear cracks; (4) delamination induced by both a bending crack and shear cracks.

$$\Pi = \sum_{m=1}^{n_{\text{ply}}} \int_{^\circ\Omega^m} W^m(E_{ij}^m)\, {}^\circ\mathrm{d}\Omega - \int_{^\circ S} {}^\circ\bar{T}_i \cdot u_i\, {}^\circ\mathrm{d}s, \tag{1}$$

where n_{ply} is the total number of layers, $^\circ\Omega^m$ is the cross-sectional area of the mth layer in the reference configuration, W is the strain energy function, u_i is the displacement vector and $^\circ S$ is the boundary in the reference configuration where the tractions $^\circ\bar{T}_i$ are applied.

The components of the second Piola–Kirchhoff stress in the mth layer can be expressed by the constitutive relation as

$$S_{ij}^m = C_{ijkl}^m E_{kl}^m, \tag{2}$$

where E_{kl}^m are the components of Green's strain tensor. C_{ijkl}^m are the orthotropic material moduli for the mth layer.

Based on the virtual work principle, the following equation can be obtained from eqn (1) for an uncracked laminate:

$$\delta\Pi = \sum_{m=1}^{n_{\text{ply}}} \int_{^\circ\Omega^m} S_{ij}^m\, \delta E_{ij}^m\, {}^\circ\mathrm{d}\Omega - \int_{^\circ S} {}^\circ\bar{T}_i \cdot \delta u_i\, {}^\circ\mathrm{d}s = 0. \tag{3}$$

The above nonlinear equation is valid for any uncracked laminated composite undergoing finite deformations in three dimensions. However, for cracked laminates, eqn (3) cannot be applied directly because of the presence of crack interfaces generated inside the materials. The contact condition of the interfacial contact during loading must be included in the analysis.

3.2. *Contact analysis*

Two types of contact are involved; the rigid–elastic contact between the indenter and the plate, and the elastic–elastic contact between the cracked/delaminated interfaces, as shown in Fig. 3. The local indentation resulting from a spherical indenter is very complicated and three-dimensional and could significantly affect the delamination growth and its interface deformation, especially when the delamination is small.

In order to prevent the contact surface from overlapping, an impenetrability condition must be specified and satisfied at all times along the contact interfaces. This condition requires that the shortest distance (defined as a gap g) between two contact surfaces be greater than, or equal to, zero. Mathematically, the impenetrability constraint can be stated as $g \geqslant 0$. Upon contact, the contact force must also be less than, or equal to, zero ($\lambda_N \leqslant 0$). Accordingly, the contact constraints for normal contact can be specified as

$$\begin{aligned} \lambda_N &\leqslant 0 \\ g(u_i) &\geqslant 0 \\ \lambda_N g(u_i) &= 0. \end{aligned} \tag{4}$$

These are the well-known Kuhn–Tucker conditions for frictionless normal contact. The three equations in eqn (4) reflect, respectively, the compressive normal traction constraint, the impenetrability constraint, and the requirement that the pressure is nonzero only when $g = 0$. Accordingly, eqn (4) must be considered together with eqn (3) in order to analyse composites containing delaminations.

It should be pointed out here that only a frictionless contact model was implemented for the present work based on the assumption that the effect of the frictional force is small. However, caution should be exercised when dealing with indentation problems for layered material systems. Recently the author investigated the microindentation process for debonded thin film systems and the material properties for debonding between the fiber and the inelastic matrix for metal matrix composite and found the friction force modeling may have a significant effect on the mechanical responses [see Liu and Zhu (1994a–c)].

Several methods exist to implement the contact constraints. The most popular choices are the Lagrange multiplier method and the penalty method. Both methods have advantages and disadvantages [see discussions in Liu (1992)]. The Lagrange multipler method was

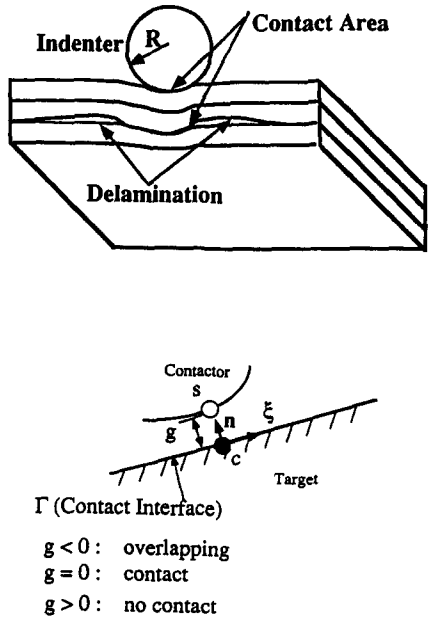

Fig. 3. Contact problem associated with a delaminated laminate subjected to an indenter. Description of local coordinates and the gap function g.

adopted previously by the author for the study of damage induced by a cylindrical indenter for analysing the interaction between matrix cracking and delamination (Liu *et al.*, 1991b, 1993). In this study, an augmented Lagrangian method was adopted. It has been shown to provide important advantages over the more traditional Lagrange multiplier and penalty methods. Detailed mathematical discussions can be found in Luenberger (1984). The augmented Lagrangian techniques have been known to provide an almost exact enforcement of constraints while using finite penalty parameters, avoiding the ill-conditioning. The application of the augmented Lagrangian techniques to contact problems has been demonstrated to be quite successful (Simo and Laursen, 1992).

In the method of augmented Lagrangians, the Lagrange multiplier λ_N is initially chosen to be an arbitrary constant. If this constant is not the correct Lagrange multiplier, the contact constraint is not satisfied and the minimization of the total potential energy of eqn (1) does not lead to the equation of equilibrium. Therefore, from a penalty function viewpoint, the total potential energy represented by eqn (1) needs to be further penalized by the following modified functional:

$$\bar{\Pi} = \Pi + \int_\Gamma \lambda_N^{(k)} g \, d\Gamma + \int_\Gamma \tfrac{1}{2}\varepsilon_N g^2 \, d\Gamma, \tag{5}$$

where $\lambda_N^{(k)} \leqslant 0$ denotes the fixed estimate of the correct λ_N. The superscript k indicates that the search for the correct λ_N is an iterative process. The updated formula is

$$\lambda_N^{(k+1)} = (\lambda_N^{(k)} + \varepsilon_N g). \tag{6}$$

Therefore, the variational equation corresponding to eqn (5) can be derived as

$$\delta\Pi + \int_\Gamma (\lambda_N^{(k)} + \varepsilon_N g)\delta g \, d\Gamma = 0. \tag{7}$$

It is noted that the term $(\lambda_N^{(k)} + \varepsilon_N g)$ plays the role of the Lagrange multiplier λ_N. If λ_N is the correct multiplier, then $g = 0$ on Γ. Thus, in the case where the multipliers are correct, eqn (7) achieves exactly the same form as the standard Lagrange multiplier method, making it an exact penalization.

It is important to notice that eqn (7) is a nonlinear equation due to the contact conditions and geometric nonlinearity. In general, then, it will be necessary to solve eqn (7) in an iterative manner. In practice, ε_N is chosen to be as large as practically possible without inducing ill-conditioning. The advantage of the current treatment over the penalty method is that satisfaction of the constraints can be improved even if ε_N is of relatively modest value through repeated application of the augmentation procedure. Since these augmentations only change $\lambda_N^{(k)}$, which is fixed with regard to solution of eqn (7), the ill-conditioning problem usually associated with the penalty method is mediated or eliminated.

A three-dimensional finite element method was developed based on eqn (7) and an eight-node brick element was used. Due to symmetry, only a quarter of the laminate was analysed.

3.3. *Failure analysis*

Because matrix cracking and delamination growth in laminated composite plates subjected to transversely concentrated loading were the major concern of the study, fiber breakage was not considered. Failure criteria were proposed for predicting the occurrence of the initial failure, and a fracture analysis based on the linear elastic fracture mechanics theory was adopted for modeling crack propagation once the damage initiated.

Prediction of initial failure. In order to predict initial damage, several existing matrix failure criteria (Gosse and Mori, 1988; Tsai and Hahn, 1975; Hashin, 1975) and a delamination failure criterion previously developed by Chang and Springer (1986), were adopted. For example, three-dimensional Hashin matrix cracking criteria can be described as

if $\sigma_{yy}+\sigma_{zz} > 0$:

$$\left(\frac{\sigma_{yy}+\sigma_{zz}}{Y_t}\right)^2+\left(\frac{\sigma_{xy}^2+\sigma_{xz}^2}{S_i^2}\right)+\left(\frac{\sigma_{yz}^2-\sigma_{yy}\sigma_{zz}}{S_i^2}\right)=e_M^2 \tag{8}$$

if $\sigma_{yy}+\sigma_{zz} < 0$:

$$\frac{\sigma_{yy}+\sigma_{zz}}{Y_t}\left(\left(\frac{Y_c}{2S_i}\right)^2-1\right)+\left(\frac{\sigma_{yy}+\sigma_{zz}}{2Y_t}\right)^2+\left(\frac{\sigma_{xy}^2+\sigma_{xz}^2}{S_i^2}\right)+\left(\frac{\sigma_{yz}^2-\sigma_{yy}\sigma_{zz}}{S_i^2}\right)=e_M^2 \tag{9}$$

Other matrix cracking criteria can be obtained in the references (Gosse and Mori, 1988; Tsai, 1975). The occurrence of matrix cracking is predicted when the value of e_M is equal to, or greater than, unity.

The delamination failure criterion can be expressed as

$$\left(\frac{\sigma_{zz}}{Y_t}\right)^2+\left(\frac{\sigma_{yz}^2+\sigma_{xz}^2}{S_i^2}\right)=e_d^2. \tag{10}$$

The occurrence of delamination at the interface is predicted when the value of e_d is equal to, or greater than, unity. In eqns (8), (9) and (10), S_i is the *in situ* interlaminar shear strength within the laminate under consideration, and Y_t and Y_c are the *in situ* ply transverse tensile and compressive strength, respectively (Liu, 1992). Also, σ_{yz} and σ_{xz} are the interlaminar shear stresses, and σ_{zz} and σ_{yy} are the out-of-plane normal stress and in-plane transverse normal stress, respectively, within the element under consideration.

Whenever the combined state of stresses satisfies either one of the criteria, initial failure was predicted. The corresponding failure criterion indicated the initial mode of failure. Once the initial failure was predicted, fracture analysis was then applied to simulate the growth of the local damage as the applied load continued to increase.

Modeling of crack propagation. The initiation of delamination growth (onset of delamination growth) was predicted based on linear elastic fracture mechanics. The well-known virtual crack closure technique by Rybicki *et al.* (1977) served as the basis for the strain energy release rate calculation. This procedure determines mode I, mode II and mode III strain energy release rates (G_I, G_{II} and G_{III}) from the energy required to close the delamination over a small area.

Therefore, at any point on the delamination front, strain energy release rates can be calculated. Since the delamination growth can be attributed to a mixed mode fracture, the criterion for determining the initiation of the delamination growth was selected as [see Liu (1992)]

$$\left(\frac{G_I}{G_{IC}}\right)^{\alpha}+\left(\frac{G_{II}}{G_{IIC}}\right)^{\beta}+\left(\frac{G_{III}}{G_{IIIC}}\right)^{\gamma}=E_d \tag{11}$$

for any point on the delamination front. Here, G_{IC}, G_{IIC} and G_{IIIC} are the critical strain energy release rates corresponding to mode I, mode II and mode III fracture, respectively. It was assumed that G_{IC}, G_{IIC} and G_{IIIC} are the critical energy release rates at the onset of the delamination growth and do not change with delamination size. Due to the fact that a sharp pre-crack is generated in regular fracture toughness testing for both mode I and II fracture toughness, the initiation value and growth value are assumed to be approximately

the same. Due to the fairly brittle property for T300/976 and quasi-static load applied, the strain rate effect is not considered for all the properties used, including the fracture toughness here. For T800H/3900-2, due to the reason that only the interface is toughened and the fairly low strain rate used on MTS machine, the material properties are assumed to be rate independent. However, care should be exercised to other impact conditions, since the dynamic response of the plate may be significantly different, as pointed out by Finn and Springer (1991). For example, Finn and Springer (1991) demonstrated that ICI APC-2 graphite-PEEK may be rate sensitive. The fracture toughness data for T300/976 has been used for delamination propagation simulation for specimens with embedded multiple through-width delaminations [see Chang and Kutlu (1989); Kutlu (1990)] and comparisons with the experimental results were excellent. Also, these same data have also been used for quasi-impact cracking initiation and induced delamination growth simulation for thin brittle laminates subjected to a cylindrical indenter/impactor [see Liu *et al.* (1991a, b, 1993)]. The subsequent three-dimensional work by Liu and Chang (1993) and Liu (1992) predicted the damage shapes and sizes with a good comparison with the measured internal delaminations and surface and internal matrix cracking by X-Ray and C-Scan. Based on the previous two-dimensional and three-dimensional studies by the author and his colleagues, $\alpha = 1$, $\beta = 1$ and $\gamma = 1$ were selected for this study, because they were found to provide the best fit to the experiments in two dimensions. It was assumed that $G_{\text{IIIC}} = G_{\text{IIC}}$ (Chai, 1989), because the value of G_{IIIC} has not been reported in the literature.

Also, due to the contact model implemented at the delamination interface, the stress oscillation may be eliminated and regular square root singularity might be maintained [see Deng (1993)]. Therefore, it is believed that the energy release rates should converge and can be used in the above criterion. Accordingly, delamination would start to propagate when $E_{\text{d}} \geqslant 1$ at any point on the delamination front.

It has to be pointed out that more accurate results could be obtained by the recently developed mixed mode fracture mechanics theory, which has been summarized in some recent review articles [see Hutchinson and Suo (1992); Shih (1991), to name a few]. Basically, two mode mixity angles ϕ and ψ_r are defined with r, indicating that ψ_r is a slowly changing function with respect to a length r. With the given mode mixity ϕ and ψ_r, the interface fracture toughness G_{c} is defined and it is a property of the bimaterial interface. For a composite interface, it is a surface in the space. The crack therefore will grow if (Shih, 1991)

$$G(\phi, \psi_r) = G_{\text{c}}(\phi, \psi_r) \tag{12}$$

at some point along the crack front.

This approach requires the fracture toughness to be determined with some length for the determination of ψ_r, which determines the relative in-plane shear to the normal tractions at that length r. However, the fracture toughness data available for the T300/976 and T800H/3900-2 were not measured according to this unique method and therefore are not considered in the current study. However, it is noted that if the mode I is zero, which occurs when some area along the crack front is in contact, only one fracture toughness is needed. This fracture toughness data happens to correspond to the case of 90° phase angle (ψ_r). When G_{I} is zero, the crack tip must be in contact due to the local feature of calculating the energy release rates by the crack tip nodal forces and the crack tip opening displacement. However, the delamination crack surface may still be partially open, which was demonstrated in the damage modes for thin laminates where the crack was mostly open due to the strong interaction between the transverse cracking and interfacial delamination.

In general, as the displacement control is used in the increment-iterative solution, it is impossible to have unity E_{d}. Therefore, the actual critical load is estimated as

$$P_{\text{cr}} = \frac{P}{E_{\text{d}}^{1/2}}, \tag{13}$$

where P_{cr} is the critical load for the given delamination to grow (corresponding to $E_{\text{d}} = 1$),

and P is the calculated applied load corresponding to the growth index E_d. It should be noted that the above equation can give fairly good results when the delamination is large and load is not big. When the delamination is small, the local geometry nonlinearity is so significant that certain error may occur. If interest is only in estimating the growth load in the linear range corresponding to a given shape and size of matrix cracks and delamination, one or two load steps can give an estimate of the critical load by the above formulae.

Numerical implementation of the failure model. Regular brick elements were used for predicting the initial damage. However, special finite element meshes were needed for studying the effect of initial damage on the delamination growth. The procedure used for generating the meshes was similar to the approaches given by Whitcomb (1988) for square plates with an elliptical delamination. However, the procedure needed here must be able to take into account rectangular plates with matrix cracking and delaminations such as the four models shown in Fig. 2. Conformal mapping was adopted to transform a circular delamination front to an elliptical one, while keeping good spacing for elements near the center. In the conformal mapping, any two lines which were orthogonal would be kept orthogonal after the mapping. Accordingly, orthogonality was well maintained in the neighborhood of the delamination front. By maintaining orthogonality, the calculation of fracture mechanics quantities such as energy release rates can be greatly simplified. A contact model was implemented along the delamination with a delicate contact search model [see Liu (1992)]. It has been observed experimentally that delamination in cross-ply composites due to low velocity impact or quasi-static indentation loading forms an ellipse-like or peanut-like shape. Therefore, only delaminations with circular or elliptical shapes were considered in the analysis, as shown in Figs 4 and 5. A typical finite element mesh is shown in Fig. 6. Details of energy release rate calculation can be found in Liu (1992).

4. RESULTS AND COMPARISON

The model was verified extensively for isotropic beams, plates and thin composite laminates both analytically and experimentally and details can be found in Liu (1992).

Damage initiation

For relatively thin composites ($[0_6/90_2]_s$, $[0_4/90_4]_s$ and $[0_2/90_6]_s$), the initial damage is matrix cracking for both T300/976 and T800H/3900-2 material systems, which has been verified experimentally (Liu, 1992). Criteria proposed by Gosse and Mori (1988), Tsai-Wu (1975) and Hashin (1975) predicted similar results. For $[(0/90)_{N/4}]_s$ layup, depending on different indenter radii, the initial damage can be the damage below the indenter or the damage inside the laminate (Fig. 7), which agrees with the experimental observation by Finn and Springer (Finn and Springer, 1991; Finn, 1991). It seems the Hashin criterion and Tsai-Wu criterion predicted correctly the initial damage mode [also see Finn (1991)]. It is explained that the global structure for thin plates are more significant and bending stress in the back surface tends to be the dominating stress component to initiate the damage. However for thicker composites, the local response due to the indenter is dominating the response. For smaller indenter, the material below the indenter tends to fail due to the highly concentrated contact load, while for bigger indenter, the transverse shear inside the material tends to cause the initial shear cracking.

Effect of fracture toughness on damage size

Both T300/976 and T800H/3900-2 composites were chosen for comparison. The stiffness and strength of unidirectional composites of both materials are similar, except for critical strain energy release rates G_{IC} and G_{IIC}. Due to its toughening interface, T800H/3900-2 composite has much higher fracture toughnesses than T300/976, especially for G_{IIC} values as shown in Table 1. Test data on T300/976 composite were taken from Finn and Springer (1991), while experiments on T800H/3900-2 composite were conducted during this investigation. Three different layups were selected; $[0_6/90_2]_s$, $[0_2/90]_s$, and $[0_4/90_4]_s$. The experiments on T800H/3900-2 composite followed the same procedures as were used by Finn

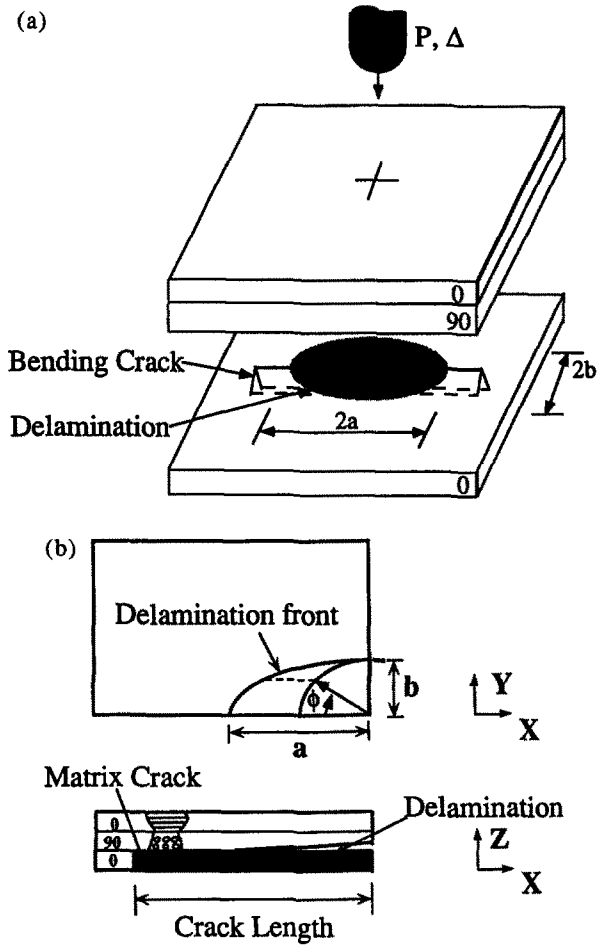

Fig. 4(a). Description of types 1 and 2 failure modes in a delaminated 0/90 composite; (b) the coordinate system used in the finite element analysis (only a quarter of the laminate is modeled).

and Springer for T300/976 composite. All the specimens had the same number of plies (16 plies), width (3 in) and length (4 in). During the tests, the specimens were clamped on the two parallel edges and free on the others. A transverse concentrated load induced through an indenter of radius 0.25 in was applied by an MTS machine. Displacement control was used throughout all the tests.

Overall the damage patterns were similar, except that the delamination sizes were substantially smaller for T800H/3900-2 composites. There was no delamination below a certain energy level in the T800H/3900-2 composites, at which the T300/976 composite had already suffered damage. At a given amount of the applied load, the damage size in the T800H/3900-2 was only about one-fifth of that observed in the T300/976. A comparison of damage size between the T300/976 and the T800H/3900-2 for various amounts of input energy is shown in Fig. 8. Figure 9 shows a comparison of critical loads for initiating delamination growth for three different delamination sizes. Figure 10 shows a typical deformation in $X-Z$, $Y=0$ cross-section of the panel due to an indentation loading.

Figure 11 presents a comparison of G/P^2 with different load levels for different delamination sizes. It seems that when delamination is larger and load is not very large, the values of G/P^2 are constant for different load levels. However, for smaller delaminations, nonlinear effects are significant and the actual increment-iterative solution needs to be used for finding the actual critical load for onset of the delamination growth. It seems that for large delaminations, one or two load steps of the linear solution may give an estimate of the critical load for the delamination growth.

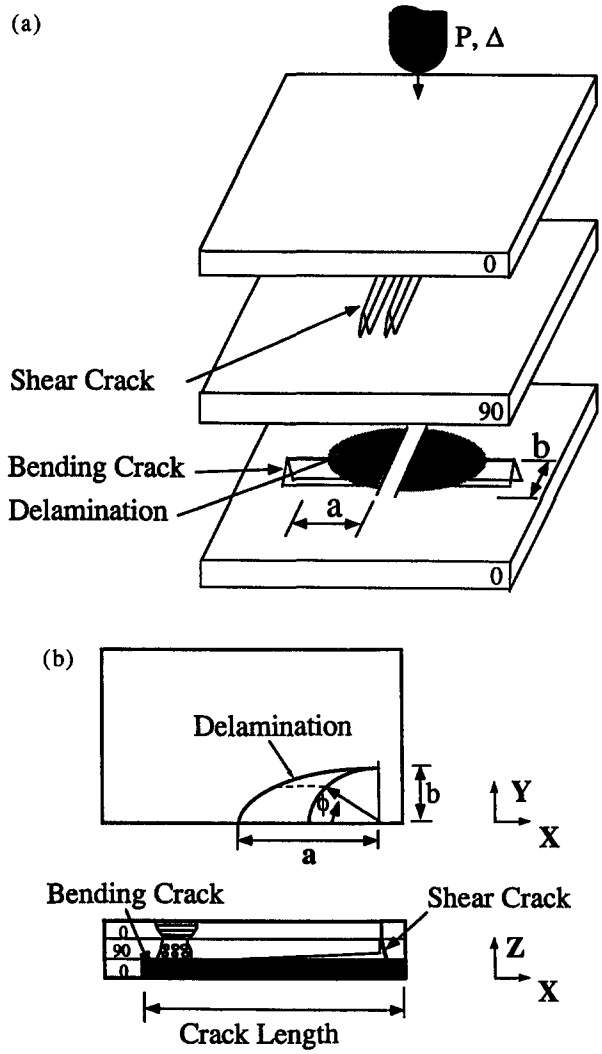

Fig. 5(a). Description of types 3 and 4 failure modes in a delaminated 0/90 composite; (b) the coordinate system used in the finite element analysis (only a quarter of the laminate is modeled).

Effect of matrix cracking on delamination growth

It has been demonstrated that matrix cracking is important to the delamination growth for thin laminates in both two and three dimensions (Liu *et al.*, 1991a, b, 1993; Liu, 1992). In the following, results are presented for a moderately thick T300/976 laminate with $[(0_3/90_3)_3]_s$ layup. Due to the fine mesh needed near the indenter and delamination front, 12 elements are used in thickness direction. The internal crack is located 0.03 in away from the center of the plate and located in the middle six 90° plies. A surface crack is assumed to occur on the back surface six plies. Four different models shown in Fig. 2 were all considered for completeness, though it is known that surface cracking is not the initial damage for the layup considered.

$[(0_3/90_3)_3]_s$ *panels with or without a surface crack.* In order to evaluate the surface matrix cracking effect on damage growth in $[(0_3/90_3)_3]_s$ composites due to transverse concentrated loading, both types 1 and 2 damage models were utilized to perform the numerical simulations. The type 1 model considered only a delamination without a bending crack, however, the type 2 model considered both the delamination and the bending crack.

Figure 12 shows a comparison of components of energy release rate normalized by the calculate load P^2 for panels containing a small delamination located on the first 0/90 counting from the bottom ply, with or without a surface crack attached to the delamination.

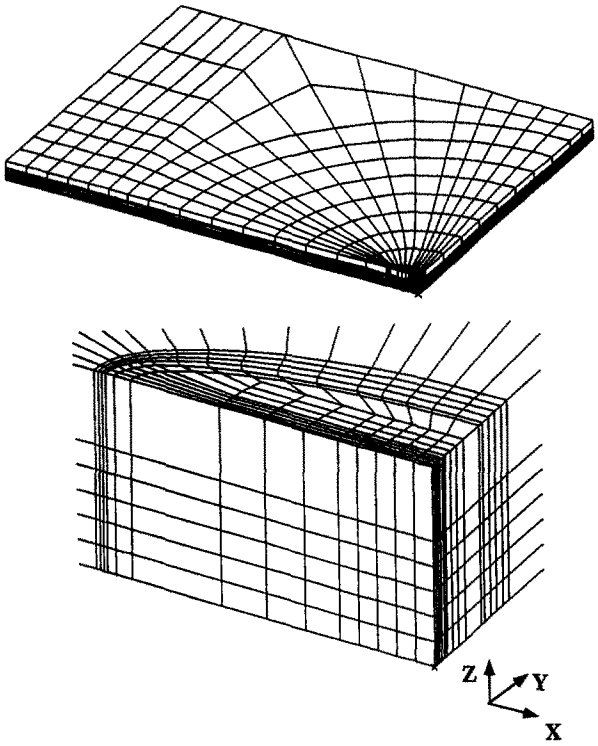

Fig. 6. Description of a typical finite element mesh used in the analysis.

The length of the bending crack is slightly larger than the delamination length due to numerical reason, although the input can be arbitrary or any measured data. The shape of the surface crack can be slender elliptical, parabolic, or rectangular and results showed that no significant difference exists in terms of energy release rate calculation. Therefore, simple rectangular shape was used in all the presented calculations. Taking into account the stiffness reduction due to the surface crack which results in smaller load P than the case without a surface crack, the bending crack effect is localized near the interaction area between the delamination and the surface crack, with main improvement in mode I component near $\phi = 0°$. This contradicts the case with thin composites (Liu *et al.*, 1993; Liu, 1992; Liu and Chang, 1993), where the surface crack significantly altered the energy release rate direction when small delamination and surface crack exist.

Figure 13 presents results for a large delamination with or without the surface crack. It is also shown that the bending effect is mainly localized near the $\phi = 0°$. Modes II and III dominate the strain energy release distribution except near $\phi = 0°$, which is also different from what was observed for thin composites [Liu *et al.*, 1993; Liu, 1992; Liu and Chang,

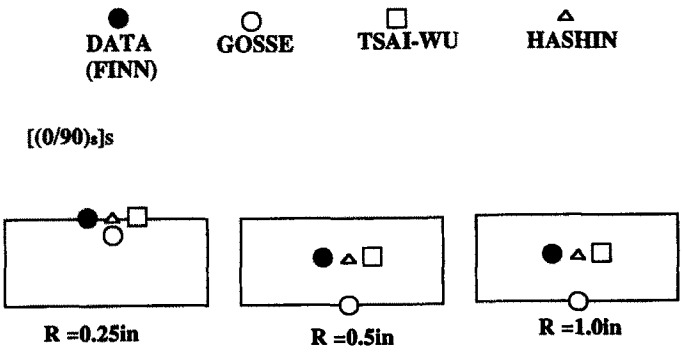

Fig. 7. Initial damage locations for three different impact nose radius.

Table 1. Material properties for T300/976 and T800H/3900-2.

Material property	T800H/3900-2	T300/976
Longitudinal Young's modulus, E_x (msi)	23.2	17.6
Transverse Young's modulus, E_y (msi)	1.33	1.41
Out-of-plane Young's modulus, E_z (msi)	1.33	1.41
Poisson's ratio, v_{xy}	0.28	0.29
Poisson's ratio, v_{xz}	0.28	0.29
Poisson's ratio, v_{yz}	0.28	0.40
In-plane shear modulus, G_{xy} (msi)	0.90	0.81
Out-of-plane shear modulus, G_{xz} (msi)	0.90	0.81
Out-of-plane shear modulus, G_{yz} (msi)	0.90	0.50
Longitudinal tensile strength, X_t (ksi)	413	220
Longitudinal compressive strength, X_c (ksi)	191	230
Transverse tensile strength, Y_t (ksi)	6.41	6.46
Transverse compressive strength, Y_c (ksi)	24.4	36.7
Longitudinal shear strength (cross-ply), S_{cp} (ksi)	52.89	15.5
Critical strain energy release rate for mode I, G_{IC} (lbf/in)	1.50	0.50
Critical strain energy release rate for mode II, G_{IIC} (lbf/in)	18.0	1.80
Ply thickness h_0 (in)	0.006535	0.0056

1993]. The explanation of the above observation is that global bending is smaller for thick composites than for thin composites. Of course, it should be pointed out that the initial damage here is not the surface crack and there does not exist any delamination induced by the surface crack. This point will be further explained when discussing the effect of shear crack on the delamination growth in the following section.

$[(0_3/90_3)_3]_s$ *panels with a shear crack and with or without a surface crack.* Both types 3 and 4 were selected to study the delamination growth behavior of $[(0_3/90_3)_3]_s$ composites, except that now in type 4 model, the surface crack on the bottom six plies is not attached to the delamination which is located at the 90/0 interface right beneath the middle six 90° plies. The length of the shear crack is also slightly larger than the y-axis of the delamination.

Figure 14 shows a comparison of components of energy release rate normalized by the calculated load P^2 for panels containing a small delamination and a shear crack attached to the delamination, with or without a surface crack located at the surface 0° plies. It was shown that the small bending crack had negligible effect on the energy release rates distribution, indicating again that the global bending effect is small. Actually, the stiffness reduction due to the surface bending crack is very small from the calculated load–displacement response. For both cases the mode I is almost zero.

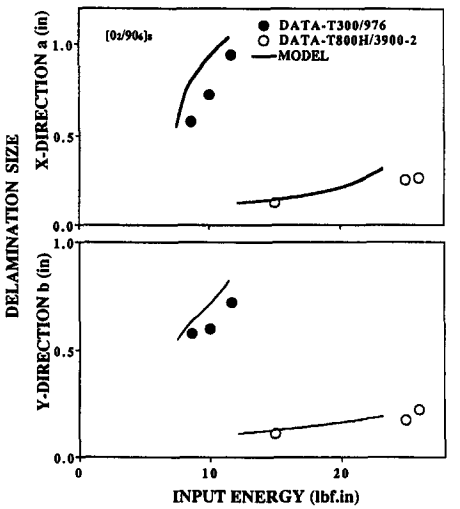

Fig. 8. Comparison between the measured and predicted delamination sizes in $[0_6/90_2]_s$ composites made of T300/976 and T800H/3900-2 with respect to quasi-impact energy.

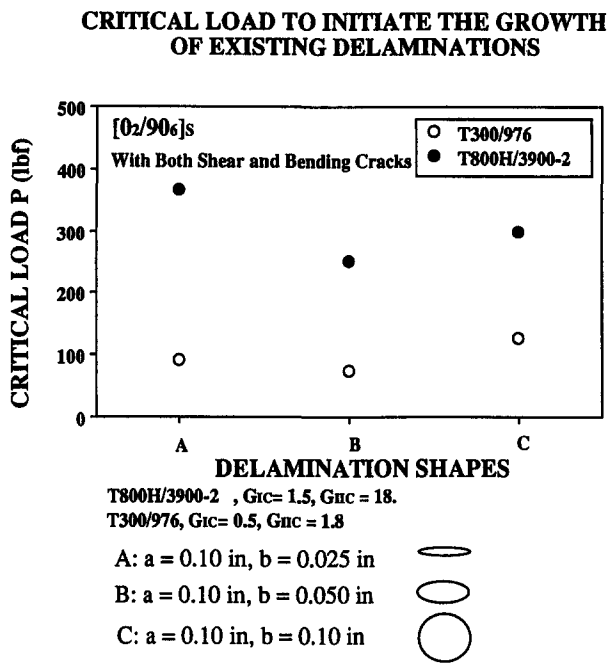

Fig. 9. Comparison between the predicted initial load for onset of delamination growth in three delaminations for composites made of T300/976 and T800H/3900-2.

As the delamination becomes larger (as shown in Figs 15 and 16), the bending crack effect is also localized near $\phi = 0°$ with a small portion of mode I in total energy release rate. This observation indicates that shear mode fracture (II and III) dominates the delamination growth for the thick-section composites considered. It is also observed that the energy release rates calculated from type 3 and 4 models are one or two orders higher than the results of type 1 and 2 models. This is not surprising, as it is shown from a different point of view that the surface crack for the considered thick-section composite cannot induce any delamination. Actually the initial damage is not the surface crack. The internal shear cracks induce a delamination and shear fracture modes II and III dominate the delamination growth for the panels considered.

Figure 17 shows schematically the contact zone distribution with different delamination sizes. When the delamination is small, the delamination is closed. When delamination becomes larger, the contact zone takes a smaller proportion of delamination area. However,

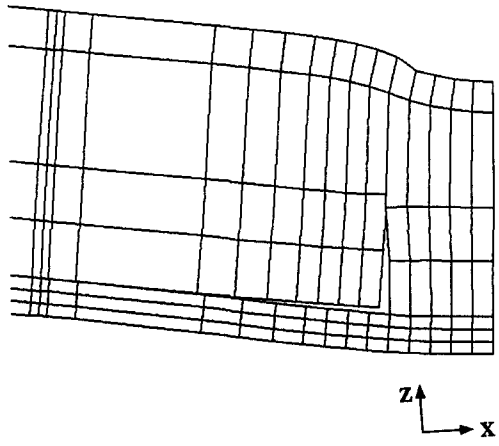

Fig. 10. Deformation of a cross-section ($X-Z$, $Y = 0$) of a composite with both a surface matrix and a pair of shear cracks.

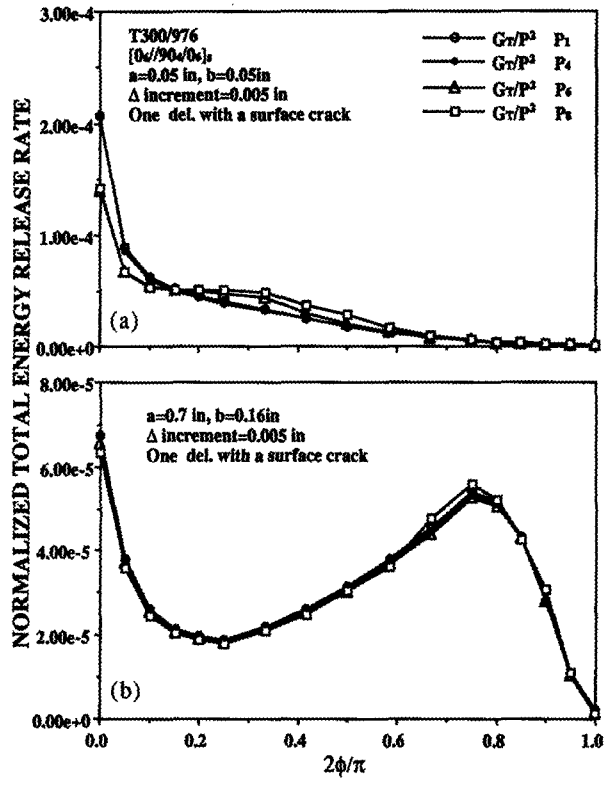

Fig. 11. The calculated total strain energy release rate along a delamination front in a T300/976 $[(0_6/90_2)_2]_s$ composite with increasing load. (a) Small delamination; (b) big delamination.

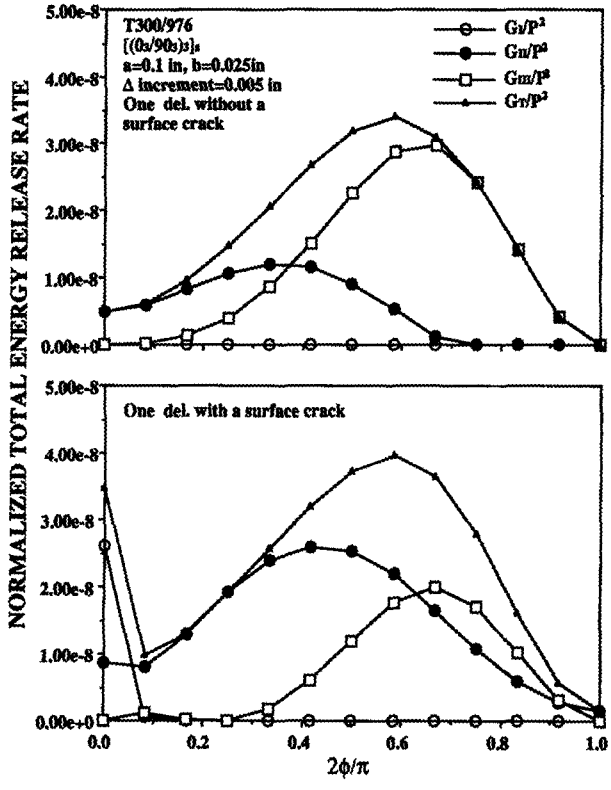

Fig. 12. Comparison of the calculated strain energy release rates of modes I, II and III along a small delamination front in a $[(0_3/90_3)_3]_s$ composite by type 1 and 2 models.

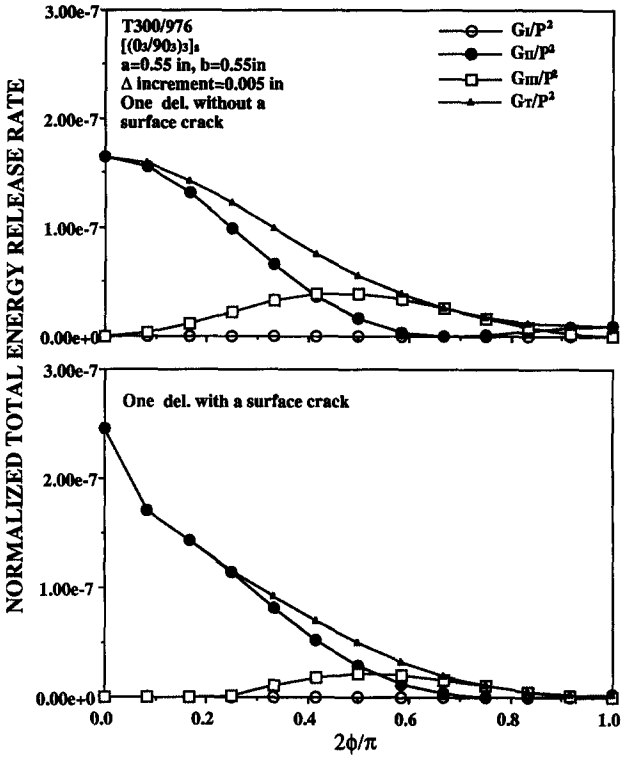

Fig. 13. The calculated strain energy release rates of modes I, II and III along a big delamination front in a $[(0_3/90_3)_3]_s$ composite by type 1 and 2 models.

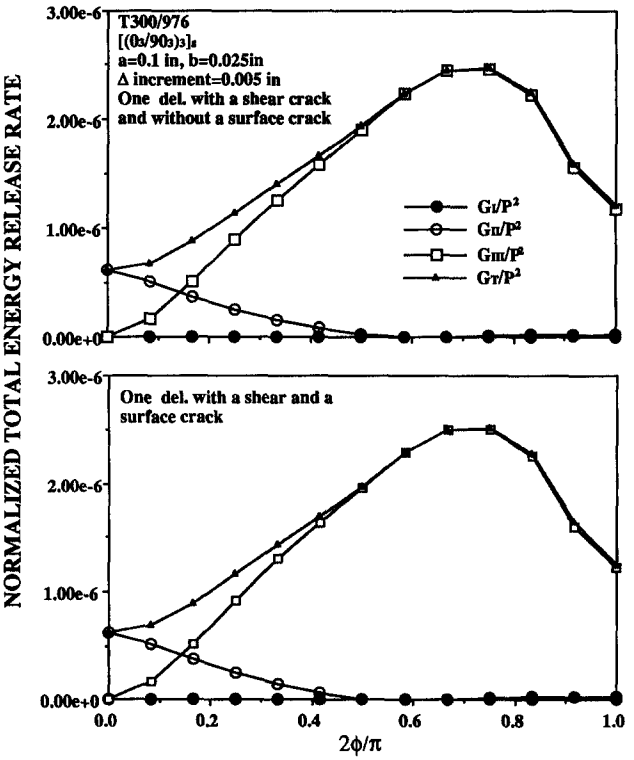

Fig. 14. Comparison of the calculated strain energy release rates of modes I, II and III along a small delamination front in a $[(0_3/90_3)_3]_s$ composite by type 3 and 4 models.

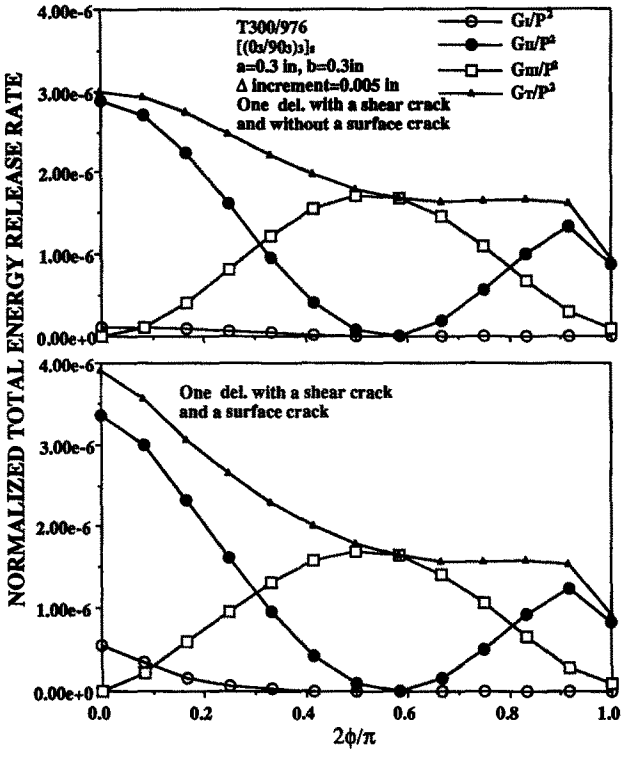

Fig. 15. The calculated strain energy release rates of modes I, II and III along a moderate delamination front in a $[(0_3/90_3)_3]_s$ composite by type 3 and 4 models.

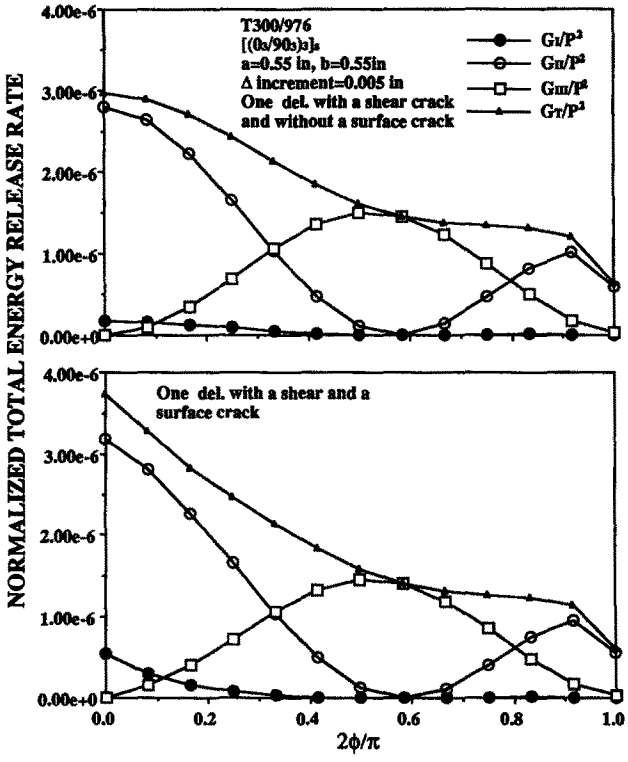

Fig. 16. The calculated strain energy release rates of modes I, II and II along a big delamination front in a $[(0_3/90_3)_3]_s$ composite by type 3 and 4 models.

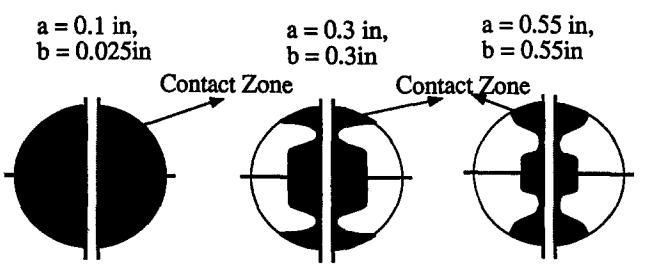

Fig. 17. Typical contact zone of a delamination in a $[(0_3/90_3)_3]_s$ composite containing an internal crack and/or a surface matrix crack.

the closed part is in significant sliding, indicating that the shear mode fracture dominates the delamination growth for the composites considered. Significant distribution of contact area also shows that the general contact algorithm has to be implemented for delamination growth.

$[(0_3/90_3)_3]_s$ *panels containing a pure delamination.* The next section addresses the question of how important it is to model the shear crack in the model for thick-section composites. The type 1 model was used to investigate this issue. Now, the delamination is located at the same interface as the type 3 model adopted. Therefore, the current model represents a compromise. That is, it does not consider the shear crack but uses one full elliptical shape (type 1 model) instead of two semi-elliptical shapes separated by a pair of shear cracks (type 3 model). Results are presented for two types of delamination which are slightly larger than those used by the type 3 model. Therefore, the delamination now is $a = 0.13$ in and $b = 0.025$ in for small delamination and $a = 0.58$ in and $b = 0.55$ in for larger delamination. Therefore the type 1 model used here should make the panel less stiff than the one modeled by the type 3 model without considering the shear crack.

Figure 18 shows energy release rate distributions for two delaminations. Compared to Figs 16 and 14, the overall energy release rates are much smaller than those cases where the shear cracks are modeled. It is also observed that the shear fracture modes still dominate the delamination growth. It is clearly indicated that the shear crack plays an important role in controlling the delamination growth and needs to be modeled in the numerical modeling, otherwise significant error may result.

5. CONCLUDING REMARKS

A model has been developed for analysing cross-ply laminated composite plates subjected to transverse concentrated loading resulting from a spherical indenter. A three-dimensional nonlinear finite element analysis was developed based on the model. Four layups and two material systems were selected for the study. Based on the analysis, the following remarks can be made for the laminates studied:

(1) the initial damage is different for thin- and thick-section composites;
(2) the initial matrix cracking significantly affects the growth of delamination resulting from transverse loading;
(3) toughened materials are significantly more damage resistant;
(4) mode II and III fracture dominate the contribution to the growth of the delamination induced by transverse loading;
(5) shear cracks have to be modeled in the fracture mechanics model in order to correctly predict the delamination growth.

Additionally, it is noted that the proposed finite element analysis can also be extended to study other ply orientations and other loading conditions, such as delamination buckling, which are going to be reported in future publications.

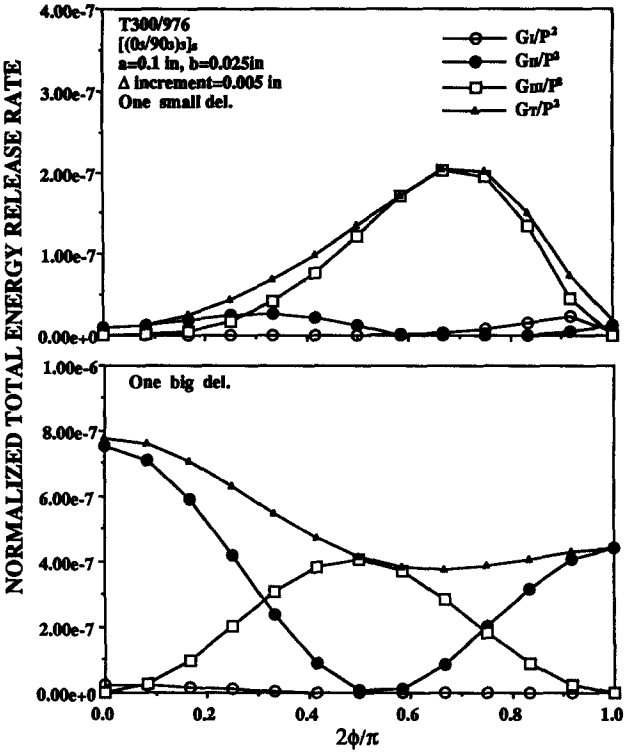

Fig. 18. Comparison of the calculated strain energy release rates of modes I, II and III along a small or big delamination front in a $[(0_3/90_3)_3]_s$ composite by type 1 model.

Acknowledgements—Part of the work presented was from the author's previous research at Stanford University and was supported by the Air Force Office of Scientific Research. The support of Professor F. K. Chang is sincerely appreciated. The discussions with Professor H. Gao of Stanford University and Professor C. W. Bert of the University of Oklahoma are gratefully appreciated. The author would like to thank two anonymous reviewers for their enlightening comments and suggestions. The numerical simulations in three-dimensional modeling were performed on the Cray Y-MP at the National Science Foundation Computing Center at the University of California, San Diego, as well as on the Cray Y-MP at Academic Computing and Network Services of Florida State University, Tallahassee.

REFERENCES

Abrate, S. (1991). Impact resistance of composite materials—a review. *Appl. Mech. Rev.* **44**, 155–190.

Benson, D. J. and Hallquist, J. O. (1990). A single surface contact algorithm for the post-buckling analysis of shell structures. *Comput. Meth. Appl. Mech. Engng* **78**, 141–163.

Cantwell, W. J. and Morton, J. (1991). Impact of laminated composite materials—a review. *Composites* **22**, 347–362.

Chai, H. (1989). Mixed-mode fracture behavior of delaminated films. *Proc. 4th Tech. Conf. Am. Soc. Composites*, pp. 815–825.

Chang, F. K. and Kutlu, Z. (1989). Collapse analysis of composite panels containing multiple delaminations. *AIAA/ASME/ASCE/AHS 30th Structures, Structural Dynamics and Materials Conference*. Mobile, AL.

Chang, F. K. and Springer, G. S. (1986). The strength of fiber reinforced composite bends. *J. Compos. Mater.* **20**(1), 30–45.

Choi, H. Y., Downs, R. J. and Chang, F. K. (1991a). A new approach toward understanding damage mechanisms and mechanics of laminated composites due to low-velocity impact. Part I—experiments. *J. Compos. Mater.* **25**(8), 992–1011.

Choi, H. T., Wu, H. Y. T. and Chang, F. K. (1991b). A new approach toward understanding damage mechanisms and mechanics of laminated composites due to low-velocity impact. Part II—analysis. *J. Compos. Mater.* **25**(8), 1012–1038.

Deng, X. (1993). Propagating interface cracks with frictionless contact. *J. Mech. Phys. Solids* **41**(3), 531–540.

Finn, S. R. (1991). Delaminations in composite plates under transverse static or impact loads. Ph.D. Thesis, Department of Aeronautics and Astronautics, Stanford University.

Finn, S. R. and Springer, G. S. (1991). *Composite Plates Impact Damage: An Atlas*. Technomic, Lancaster, PA.

Gosse, J. H. and Mori, P. B. Y. (1988). Impact damage characterization of graphite/epoxy laminates. *Proc. 3rd Tech. Conf. American Soc. Composites*, pp. 334–353. Seattle, WA.

Greszczuk, L. B. (1973). Foreign objects damage to composites. ASTM STP 568.

Gu, Z. L. and Sun, C. T. (1987). Prediction of impact damage region in SMC composites. *Compos. Struct.* **7,** 179–190.

Hashin, Z. (1975). Failure criteria for unidirectional fiber composites. *J. Appl. Mech.* **47,** 329–334.

Hutchinson, J. W. and Suo, Z. (1992). Mixed mode cracking in layered materials. *Adv. Appl. Mech.* **29,** 63–191.

Jones, S., Paul, J., Tay, T. E. and Williams, J. F. (1988). Assessment of the effect of impact damage in composites: some problems and answers. *Compos. Struct.* **10,** 51–73.

Joshi, S. P. and Sun, C. T. (1986). Impact-induced fracture in quasi-isotropic laminate. *J. Compos. Tech. Res.* **19,** 40–46.

Kutlu, Z. (1990). Compression response of laminated composite panels containing multiple delaminations. Ph.D. Thesis, Department of Mechanical Engineering, Stanford University.

Lawry, M. H. (1990). I-DEAS Student Guide, Structural Dynamics Research Corporation. Milford, OH.

Liu, D. and Malvern, L. E. (1987). Matrix cracking in impacted glass/epoxy plates. *J. Comput. Struct.* **21,** 594–609.

Liu, S. (1992). Damage mechanics of cross-ply laminated composites resulting from transverse concentrated loading. Ph.D. Thesis, Department of Mechanical Engineering, Stanford University.

Liu, S. and Chang, F. K. (1993). Matrix cracking effect on delamination growth in laminated composites induced by a spherical indenter. *J. Compos. Mater.* (in press).

Liu, S. and Zhu, J. S. (1994a). Effective moduli of unidirectional fiber composites containing radial cracking and interfacial debonding. *Int. J. Damage Mech.* (in press).

Liu, S. and Zhu, J. S. (1994b). Elastic–plastic finite element models for microindentation of thin film substrate systems with debonding. *J. Mater. Res.* (submitted).

Liu, S. and Zhu, J. S. (1994c). Contact and fracture modeling of debonded thin film layered systems due to the microindentation. *Int. J. Solids Structures* (submitted).

Liu, S., Kutlu, Z. and Chang, F. K. (1991a). Matrix cracking and delamination in laminated polymeric composites resulting from transversely concentrated loadings. *Proc. 1st Int. Conf. Deformation Fract. Composites*, pp. 30/1–30/7. Manchester, U.K.

Liu, S., Kutlu, Z. and Chang, F. K. (1991b). Matrix cracking-induced stable and unstable delamination propagation in graphite/epoxy laminated composites due to quasi-static transverse concentrated load. *4th Symp. Composite Mater. Fatigue Fract. STP 1156.*

Liu, S., Kutlu, Z. and Chang, F. K. (1993). Matrix cracking and delamination propagation in laminated composite subjected to transversely concentrated loading. *J. Compos. Mater.* **27**(5), 436–470.

Lu, X. and Liu, D. (1989). Strain energy release rates at delamination front. *Proc. 4th Tech. Conf. Am. Soc. Composites*, pp. 277–286.

Luenberger, D. G. (1984). *Linear and Nonlinear Programming.* Addison-Wesley, Reading, MA.

Malvern, L. E., Sierakowski, R. L., Ross, L. A. and Cristescu, N. (1978). Impact failure mechanisms in fiber-reinforced composite plates. In *High Velocity Deformation of Solids* (Edited by Kawata and Shiori), pp. 120–130. Springer-Verlag, Berlin.

Martin, R. H. and Jackson, W. C. (1991). Damage prediction in cross-plied curved composite laminates. NASA Technical Memorandum 104089.

Odagiri, N., Kishi, H. and Nakae, T. (1989). T800H/3900-2 toughened epoxy prepreg system; toughening concepts and mechanism. *34th Int. SAMPE Symp.*, pp. 43–52.

Poe, C. C., Jr (1988). Simulated impact damage in a thick graphite/epoxy laminate using spherical indenters. NASA TM-100539.

Rybicki, E. F. and Kanninen, M. F. (1977). A finite element calculation of stress intensity factors by a modified crack closure integral. *Engng Fract. Mech.* **9,** 931–938.

Salpekar, S. A. (1991). Analysis of delamination in cross ply laminates initiating from impact induced matrix cracking. NASA Contract Report 187594.

Shih, C. F. (1991). Cracks on bimaterial interfaces: elasticity and plasticity aspects. *Mater. Sci. Engng* **A143,** 77–90.

Simo, J. C. and Laursen, T. A. (1992). An augmented Lagrangian treatment of contact problems involving friction. *Comput. Struct.* **42**(1), 97–116.

Sjöblom, P. O., Hartness, J. T. and Cordell, T. M. (1988). On low-velocity impact testing of composite materials. *J. Compos. Mater.* **22,** 30–52.

Sun, C. T. and Manoharan, M. G. (1989). Growth of delamination cracks due to bending in a $[90_5/0_5/90_5]$ laminate. *Compos. Sci. Tech.* **34,** 365–377.

Tsai, S. W. and Hahn, H. T. (1975). *Introduction to Composite Materials.* Technomic, Lancaster, PA.

Whitcomb, J. D. (1988). Instability-related delamination growth of embedded and edge delaminations. NASA Technical Memorandum 100655.

Wu, H. T. and Springer, G. S. (1988a). Measurements of matrix cracking and delamination caused by impact on composite plates. *J. Compos. Mater.* **22,** 518–532.

Wu, H. T. and Springer, G. S. (1988b). Impact induced stresses, strains and delaminations in composite plates. *J. Compos. Mater.* **22,** 533–560.